# Effects of neutron-star dynamic tides on gravitational waveforms within the effective-one-body approach

Tanja Hinderer,[1,2] Andrea Taracchini,[2] Francois Foucart,[3] Alessandra Buonanno,[2] Jan Steinhoff,[2,4] Matthew Duez,[5] Lawrence E. Kidder,[6] Harald P. Pfeiffer,[7] Mark A. Scheel,[8] Bela Szilagyi,[9,8] Kenta Hotokezaka,[10] Koutarou Kyutoku,[11] Masaru Shibata,[12] and Cory W. Carpenter[5]

[1]*Department of Physics,University of Maryland, College Park, MD 20742, USA*
[2]*Max Planck Institute for Gravitational Physics (Albert Einstein Institute), Am Mühlenberg 1, Potsdam-Golm, 14476, Germany*
[3]*Lawrence Berkeley National Laboratory, 1 Cyclotron Rd, Berkeley, CA 94720, USA; Einstein Fellow*
[4]*Centro Multidisciplinar de Astrofísica, Departamento de Física, Instituto Superior Técnico, Universidade de Lisboa, Avenida Rovisco Pais 1, 1049-001 Lisboa, Portugal*
[5]*Department of Physics & Astronomy, Washington State University, Pullman, Washington 99164, USA*
[6]*Cornell Center for Astrophysics and Planetary Science, Cornell University, Ithaca, NY 14853 USA*
[7]*Canadian Institute for Theoretical Astrophysics, University of Toronto, Toronto, Ontario M5S 3H8, Canada*
[8]*Theoretical Astrophysics 350-17, California Institute of Technology, Pasadena, CA 91125, USA*
[9]*Jet Propulsion Laboratory, California Institute of Technology, 4800 Oak Grove Dr. Pasadena CA, 91109, USA*
[10]*Racah Institute of Physics, The Hebrew University of Jerusalem, Jerusalem, 91904, Israel*
[11]*Interdisciplinary Theoretical Science (iTHES) Research Group, RIKEN, Wako, Saitama 351-0198, Japan*
[12]*Yukawa Institute for Theoretical Physics, Kyoto University, Kyoto 606-8502, Japan*

(Dated: February 2, 2016)

Extracting the unique information on ultradense nuclear matter from the gravitational waves emitted by merging, neutron-star binaries requires robust theoretical models of the signal. We develop a novel effective-one-body waveform model that includes, for the first time, *dynamic* (instead of only adiabatic) tides of the neutron star, as well as the merger signal for neutron-star–black-hole binaries. We demonstrate the importance of the dynamic tides by comparing our model against new numerical-relativity simulations of nonspinning neutron-star–black-hole binaries spanning more than 24 gravitational-wave cycles, and to other existing numerical simulations for double neutron-star systems. Furthermore, we derive an effective description that makes explicit the dependence of matter effects on two key parameters: tidal deformability and fundamental oscillation frequency.



*Introduction.* Neutron stars (NSs) represent the strongest gravitational environment where matter can stably exist, with central densities several times higher than the density of an atomic nucleus ($\sim 3\times10^{14}\,\mathrm{g\,cm^{-3}}$) and $\sim 10^{13}$ times larger than the central density of the Sun. Under such great compression the ordinary structure of nuclear matter completely disintegrates; instead, novel phases of matter, new particles, or deconfined quarks may appear. The composition and nature of the ultradense NS matter encoded in its equation of state (EoS) remains a longstanding frontier in physics, despite recent constraints [1, 2]. However, upcoming observations of gravitational waves (GWs) from merging NS-NS or NS-black hole (BH) binaries with ground-based interferometers (advanced LIGO [3], advanced Virgo [4], and KAGRA [5]) will have a unique potential to probe the NS EoS, and possibly to combine this information with that obtained from associated electromagnetic transients [6].

Yet, the success of extracting the EoS information from the noisy data is contingent upon highly accurate theoretical waveform models (templates) for matched-filtering data analysis, where the datastream is cross-correlated with a bank of templates covering the entire physical parameter space. Building sufficiently accurate GW templates requires a detailed physical understanding of the influence of NS matter on the signal. This is a challenging problem due to the diverse phenomenology resulting from systems with different parameters (EoS, masses, spins, microphysics, or magnetic fields) [7–11].

During the binary's gradual inspiral epoch, a small but clean signature of the NS matter arises from tidal interactions [12–18], when the gravity gradient across the NS causes it to deform away from sphericity, similar to the Earth's tidal bulges. The dominant imprint in the GWs is due to the NS's *adiabatic* tide (AT), where the distorted NS remains in hydrostatic equilibrium and, in the absence of dissipation, adjusts instantaneously to the companion's tidal force which varies periodically due to the orbital motion. The AT is characterized by a single constant for each multipole: the neutron star's tidal deformability, or Love number [19]. This parameter contains key information on the NS's interior similar to the Love number measured for Saturn's moon Titan from Cassini flyby data which revealed the likely existence of a subsurface ocean [20].

In this paper we advance the modeling of NS tidal interactions by computing *dynamical* tidal effects in a binary inspiral and demonstrating their importance for accurate GW templates. Dynamic tides (DTs) arise when the frequency of the tidal forcing comes close to an eigenfrequency of the NS's normal modes of oscillation (standing wave patterns), resulting in an enhanced and more complex tidal response than in the adiabatic case. Normal modes of NSs carry detailed information about their interiors, akin to the oscillations of the Earth excited by earthquakes that are used in seismology to probe the Earth's structure. We will focus here on the modes with the strongest tidal coupling, namely the fundamental modes of oscillation ($f$-modes) describing the NS's quadrupole ($\ell=2$) degrees of freedom. They behave like harmonic oscillators driven by a periodic force whose amplitude

and frequency are slowly varying. This is a well-studied general problem and, in the context of Newtonian tidal interactions for nonspinning bodies on circular orbits, is described by the Lagrangian [14, 16]

$$L_{\rm Q} = \sum_{m=-\ell}^{\ell} \left[ -\frac{1}{2} Q_m E_m e^{-im\phi(t)} + \frac{1}{4\lambda\omega_f^2} \left( \dot{Q}_m^2 - \omega_f^2 Q_m^2 \right) \right]. \tag{1}$$

Here, the $Q_m$'s are the quadrupole modes, overdots denote time derivatives, the $E_m$'s are the amplitudes of the tidal field, $\phi(t) = \int \Omega \, {\rm d}t$ is the orbital phase, and $\lambda$ is the tidal deformability. Gravitational radiation reaction (RR) effects cause the orbital frequency $\Omega$ and $E_m$ to slowly evolve. The Euler-Lagrange equations for (1) have the static solution $Q_0 = -\lambda E_0$ and, in the AT approximation where $\omega_f \gg |m|\Omega$, the other modes are simply $Q_m^{\rm AT} = -\lambda E_m e^{-im\phi}$. By contrast, the approximate dynamical behavior calculated from a two-timescale expansion [21] is

$$\frac{Q_m^{\rm DT}}{Q_m^{\rm AT}} \approx \frac{\omega_f^2}{\omega_f^2 - (m\Omega)^2} + \frac{\omega_f^2}{2(m\Omega)^2 \varepsilon_f \Omega_f' (\phi - \phi_f)} \pm \frac{i\omega_f^2}{(m\Omega)^2\sqrt{\varepsilon_f}} e^{\pm i\Omega_f' \varepsilon_f (\phi-\phi_f)^2} \int_{-\infty}^{\sqrt{\varepsilon_f}(\phi-\phi_f)} e^{\mp i\Omega_f' s^2} {\rm d}s. \tag{2}$$

Here, the upper sign is for $m > 0$, the lower sign for $m < 0$ and the subscript $f$ indicates evaluation at the resonance where $|m|\Omega(t_f) = \omega_f$, i.e., when the tidal driving force becomes phase coherent with the $f$-modes. Also, $\varepsilon_f = \Omega^{-1}/t_{\rm RR}$ is the ratio between the orbital and RR timescales and $\Omega_f'$ is a (rescaled) derivative of $\Omega$. The first term in Eq. (2) is an equilibrium solution that causes an increasing correction to $Q_m^{\rm AT}$ already long before the resonance. Its divergent denominator is canceled by the additional term in the first line, while the Fresnel integral in the last line of Eq. (2) captures the near-resonance dynamics. The solution in Eq. (2) is finite and valid for frequencies up to $\omega_f + \mathcal{O}(\sqrt{\varepsilon_f})$; we omit the post-resonance terms here since for nonspinning binaries $\omega_f$ becomes $\sim |m|\Omega$ only close to the merger for low $\ell$-poles.

Aside from a few exceptions [14–16, 22–24], most previous studies were motivated by the fact that for low multipoles $\omega_f > |m|\Omega$ during most of the inspiral, so they focused on the adiabatic limit $\omega_f/(|m|\Omega) \to \infty$. However, as we will demonstrate below, depending on the system parameters, the finite frequency contributions illustrated in Eq. (2) can become appreciable and must be included in robust GW template models. The aim of this paper is to develop such physically more accurate GW templates for EoS measurements with the upcoming GW observations. While the main impact of our model is on templates for NS-NS binaries, here we focus our assessments primarily on NS-BH binaries with low mass ratios, which, although less likely as astrophysical sources, currently enable the most accurate tests of the model against numerical-relativity (NR) results.

*Effective-one-body (EOB) model with dynamic tides.* The EOB framework [25–29] combines perturbative results from the weak-field post-Newtonian (PN) approximation, valid for any mass ratio, but limited to mildly relativistic motion, with strong-field effects from the test-particle limit. These results are resummed in an appropriate Hamiltonian, RR force and GW polarizations, and further improved by calibrating parameterized higher-order PN terms to NR data. This yields a highly accurate model that has been very succesful in describing the entire signal from BH-BH systems [27–29].

Specifically, using geometric units $G = 1 = c$, and setting $M = m_1 + m_2$ and $\nu = m_1 m_2/M^2$, where $m_1$ and $m_2$ are the compact-objects' masses, the conservative dynamics of the binary is described by the Hamiltonian $H_{\rm EOB} = M\sqrt{1 + 2\nu\,(H_{\rm eff}/\mu - 1)} - M$, where $H_{\rm eff}$ is the Hamiltonian of an effective test-particle of mass $\mu \equiv \nu M$ moving in the effective metric ${\rm d}s^2 = -A\,{\rm d}t^2 + A^{-1}D\,{\rm d}r^2 + r^2({\rm d}\theta^2 + \sin^2\theta\,{\rm d}\phi^2)$, with $A$ and $D$ being certain potentials that we discuss below. In the nonspinning case, the motion is in a plane ($\theta = \pi/2$) and the effective Hamiltonian is

$$H_{\rm eff} = \sqrt{A}\sqrt{\mu^2 + \frac{p_\phi^2}{r^2} + \frac{p_r^2}{AD} + 2(4-3\nu)\frac{p_r^4}{\nu r^2}}, \tag{3}$$

where $p_\phi$ and $p_r$ are the canonical azimuthal angular and radial momentum. Adopting the subscript "PP" to emphasize that the expression applies to the point-particle case (i.e., tidal effects set to zero), we use for the potential $A_{\rm PP}$ the function $\Delta_u$ given in Eq. (2) of Ref. [27] with the calibration parameters determined therein and the spins set to zero, and take $1/D_{\rm PP}$ from Eq. (10) of Ref. [30]. Adiabatic tidal effects have also been included in the EOB model [18, 31, 32].

Here, we devise a novel tidal EOB (TEOB) model that includes DT effects. We derive the Hamiltonian from the Lagrangian (1) plus its 1PN extension from Ref. [33] and the PP contributions, perform a canonical transformation to EOB coordinates, and implement several EOB resummations of the tidal terms [34]. We consider here the choice where the tidal terms are assigned to different parts of $H_{\rm eff}$ according to their nature: tidal interaction terms not involving any momenta are included by replacing in Eq. (3) $A$ with $A_{\rm PP} + A_{\rm DT}$, interaction terms involving the orbital momenta and the oscillator's kinetic and elastic energy are included by setting $\mu^2 \to \mu^2 + \mu^2_{\rm DT}$, and effects arising from using a noninertial reference frame and relativistic frame dragging are added linearly to Eq. (3) through a term $f_{\rm DT}$. Specifically,

$$A_{\rm DT} = \mathscr{E}_{ij} Q^{ij}, \quad f_{\rm DT} = -Z\, \boldsymbol{S}_Q \cdot \boldsymbol{\ell} \tag{4a}$$

$$\mu^2_{\rm DT} = \frac{z}{2\mu\lambda}\left( Q_{ij}Q^{ij} + 4\lambda\omega_f^2 P_{ij}P^{ij} \right) + Q_{ij}\mathscr{C}^{ij}, \tag{4b}$$

where $Q_{ij} = \sum_m \mathscr{Y}^{2m}_{ij} Q_m$ and $\mathscr{Y}^{2m}_{ij}$ are symmetric trace-free tensors [35], $P_{ij}$ is the momentum conjugate to $Q_{ij}$, $\mathscr{E}_{ij}$ and $\mathscr{C}^{ij}$ describe the couplings to the orbital motion, $S^i_Q = 2\varepsilon_{ijk} Q_{nj} P^{kn}$ is the angular momentum associated with the quadrupole, and $\boldsymbol{\ell} = \boldsymbol{x} \times \boldsymbol{p}/|\boldsymbol{x} \times \boldsymbol{p}|$ is a unit vector along the orbital angular momentum. For circular orbits and for $Q_{ij}$ expressed in a frame that is co-rotating with the orbital motion

we obtain [34]

$$\mathscr{E}_{ij} = -\frac{3m_2}{\mu r^3} n^i n^j \left[1 - \frac{2m_2-\mu}{r} + \frac{5m_1(33m_1-7M)}{28r^2}\right],$$
$$Z = \frac{\sqrt{M}}{\mu r^{3/2}}\left[1 - \frac{3m_2+\mu}{2r} - M\frac{m_2(9-6\nu)+\mu(27+\nu)}{8r^2}\right],$$
$$z = 1 + \frac{3m_1}{2r} + \frac{27Mm_1}{8r^2}, \quad \mathscr{C}^{ij} = \frac{3m_2}{\nu r^4}\left(\ell^i\ell^j + \nu n^i n^j\right), \tag{4c}$$

where $m_1 = m_{\rm NS}$, $m_2 = m_{\rm BH}$. In the case where both bodies are NSs, one must add to Eq. (4) the same expression with $m_1 \leftrightarrow m_2$ and the values of $\{\lambda, \omega_f\}$ for the companion. In Eq. (4) only the 1PN information is complete, since the 2PN Lagrangian is only known in the AT limit. We have included this partial 2PN information in Eq. (4) by matching the 2PN AT potential from Eqs. (6.9) and (6.10) of Ref. [31] to $\mathscr{E}_{ij}$, using the 2PN accurate redshift $z$ given in Eq. (6.3) of [31], and deriving the 2PN contribution to $Z$ from Eqs. (3.13) of Ref. [36]. To quantify the uncertainty due to the lack of high-order PN information on DT effects we also examine two alternative choices for including tidal effects in the Hamiltonian (3), namely by including all the tidal terms either in $A_{\rm DT}$ or in $\mu^2_{\rm DT}$, as discussed in Ref. [34].

The TEOB equations of motion are

$$\frac{{\rm d}x^i}{{\rm d}t} = \frac{\partial H_{\rm EOB}}{\partial p_i}, \quad \frac{{\rm d}p_i}{{\rm d}t} = -\frac{\partial H_{\rm EOB}}{\partial x^i} + \mathscr{F}_i \tag{5a}$$
$$\frac{{\rm d}Q^{ij}}{{\rm d}t} = \frac{\partial H_{\rm EOB}}{\partial P_{ij}}, \quad \frac{{\rm d}P_{ij}}{{\rm d}t} = -\frac{\partial H_{\rm EOB}}{\partial Q^{ij}} + \mathscr{F}_{ij}, \tag{5b}$$

where the $\mathscr{F}$'s are the RR forces constructed from the GW modes $h^{lm}$ in the form $\mathscr{F}(h^{lm}) = \mathscr{F}(h^{lm}_{\rm PP} + h^{lm}_{\rm DT})$. Here, we use in Eq. (5a) the approximation $\mathscr{F}_i = \mathscr{F}_i(h^{lm}_{\rm PP} + h^{lm}_{\rm AT})$ computed from Eqs. (12) and (13) of Ref. [30] with $h^{lm}_{\rm PP}$ from Eq. (4) from Ref. [30] and $h^{lm}_{\rm AT}$ from Eqs. (A14)–(A17) of Ref. [37] (but including only those PN orders where the analytical knowledge is complete). For the force on the oscillators in Eq. (5b) we approximate $\mathscr{F}_{ij} \approx 0$. We also change from $p_r$ to a new variable $p_{r*}$ as in Ref. [30]. The initial conditions for the six degrees of freedom in $Q_{ij}$ and $P_{ij}$ are the equilibrium solutions to Eqs. (5b) for circular orbits.

*Effective TEOB model.* We next provide an approximate but more efficient description of DT effects for use in practical implementations. This is accomplished by setting in Eq. (3) $A = A_{\rm PP} + A^{\rm eff}_{\rm AT}$, where the function $A^{\rm eff}_{\rm AT}$ is obtained by replacing in Eqs. (6.9) and (6.10) of Ref. [31] the constant Love numbers $k_\ell$ by $k^{\rm eff}_\ell$ given by

$$k^{\rm eff}_\ell = k_\ell\left[a_\ell + b_\ell \frac{\omega_f^2}{2(m\Omega)^2}\left(\frac{Q^{\rm DT}_{m=\ell}}{Q^{\rm AT}_{m=\ell}} + \frac{Q^{\rm DT}_{m=-\ell}}{Q^{\rm AT}_{m=-\ell}}\right)\right]. \tag{6}$$

The quantities $Q_m$ are given explicitly in Eq. (2), and the coefficients $a_\ell$ and $b_\ell$, which arise from the relative factors between $E_{m\neq\ell}$ and $E_{m=\ell}$, have the values $\{a_2,\ b_2\} = \{1/4,\ 3/4\}$ and $\{a_3,\ b_3\} = \{3/8,\ 5/8\}$ [1]. We express $k^{\rm eff}_\ell$ entirely as a function of $r$ and the binary's parameters by substituting in Eq. (2) the results for a Newtonian point particle inspiral, for which $\Omega^2 = M/r^3$, $(\phi - \phi_f) = (32M^{3/2}\mu)^{-1}[(\sqrt{M}|m|\omega_f)^{5/3} - r^{5/2}]$, $\Omega' = 3/8$, and $\varepsilon_f = 256M^{2/3}\omega_f^{5/3}\mu/(5|m|^{5/3})$. The behavior of $k^{\rm eff}_\ell$ is illustrated in Fig. 1; see Refs. [38, 39] for other work on an effective tidal response. The first peak in $k^{\rm eff}_\ell$ corresponds to the location of the resonance which excites a free oscillation that subsequently dephases from the tidal driving force, thus leading to a reduction of the net strength of the tidal interaction. The result (6) captures the DT effects very well, with the discrepancies to full DT evolutions being smaller than the uncertainty in the DT model due to the lack of 2PN information. It follows from Eqs. (2) and (6) that for $\ell = 2$ the maximum amplitude of the DT effect, if attained before the inspiral terminates, scales as $\sim C_{\rm NS}^{-5/6}(1+q)^{1/6}/\sqrt{q}$ (where $C_{\rm NS}$ is the compactness of the NS), indicating that DT effects are most important for low mass ratios.

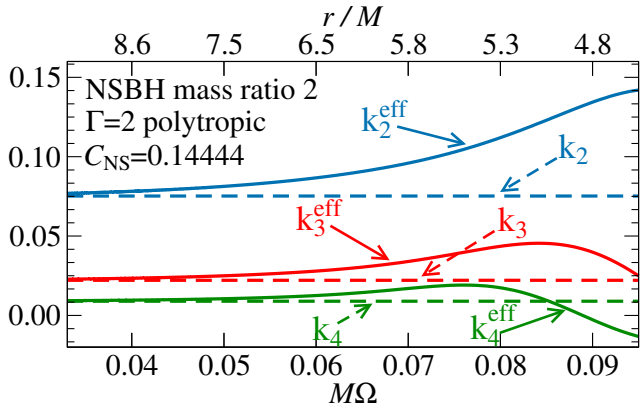


FIG. 1. **Effective dimensionless tidal coefficient for DT effects** (solid lines) and the adiabatic constant values (dashed lines) as functions of the orbital frequency $\Omega$ and relative separation $r$. The first peak in each solid line corresponds to the occurrence of the mode resonance.

*NS-BH merger model.* We complete the TEOB full waveform model by including modifications for the NS-BH merger, when the NS either plunges into the BH or it is tidally disrupted when the BH's tidal force overcomes the NS's self-gravity. The latter produces a prominent EoS-dependent damping in the GW signal [40, 41] which has been incorporated in state-of-the-art phenomenological models [42, 43]. The NR simulations for $C_{\rm NS} = 0.1444$ reveal that for $q = \{1, 1.5, 2\}$ the NS is strongly disrupted as marked by a sudden decrease in its central density which corresponds to the peak in the GW amplitude at a time $t^A_{\rm peak}$. Also, the GW frequency reaches a peak at time $t^\omega_{\rm peak}$, with $t^A_{\rm peak} < t^\omega_{\rm peak}$.

[1] For $\ell > 2$, resonances with $|m| < \ell$ are neglected since they occur at higher frequencies and thus have only a minor influence on the dynamics

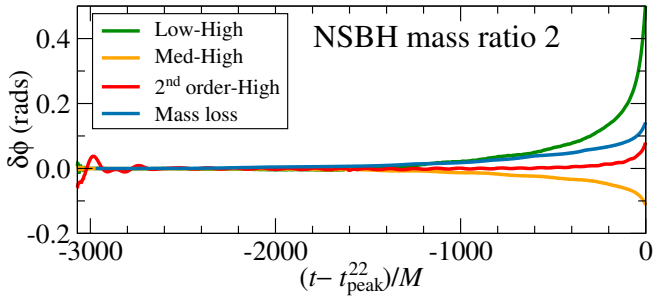


FIG. 2. **Error budget for NS-BH NR simulations**. We show for $q=2$ the phase differences $\delta\phi$ with respect to the highest resolution simulation available using HO methods to quantify the sources of error due to finite resolution and mass escaping from the grid.

We model the signal for $t \geq t^{A}_{\rm peak}$ using fits of the NR amplitude $|h_{22}|$ and frequency $\omega_{22}$ with fitting functions of the form $|h_{22}|_{\rm fit} = A_0/\cosh(A_1\tilde{t}_A + A_2\tilde{t}_A^2)$ and $\omega_{22}^{\rm fit} = (B_0 + B_1\tilde{t}_\omega)/\cosh(B_2 + B_3\tilde{t}_\omega + B_4\tilde{t}_\omega^2)$. Here, $\tilde{t}_{A,\omega} \equiv t - t^{A,\omega}_{\rm peak}$ and $A_i$ and $B_i$ are fitting parameters subject to constraints that aid in the convergence of the fitting algorithm. The parameters $A_i$ and $B_i$ are fitted with interpolating polynomials in $q \in [1,2]$. The fits are smoothly connected to the inspiral portion of the signal via blending functions of the form $[1+\exp(\pm\tilde{t}_A/w)]^{-1}$, where $w$ relates to the width of the transition region.

*Accuracy of the TEOB model.* The TEOB model relies on several approximations, however, we checked that the DTs dominate over other physical effects. Specifically, we verified that the effects on the GW phase of a nonlinear tidal response and nonlinear couplings are a few % at most, excluding the immediate vicinity of the tidal disruption. Moreover, we found that higher multipoles $\ell > 3$ lead to corrections $\lesssim 0.02$ rads over 24 GW cycles, based on the hexadecapole. The inclusion of the DT effects into the $h^{lm}$ modes is the subject of future work; using an effective description we find indications that this will amplify the net effect in the GW signal but making a smaller contribution than the DTs in the conservative dynamics. Finally, the approximation $\mathscr{F}_{ij} \approx 0$ showed a negligible influence on the phase over 24 GW cycles in a Newtonian inspiral code.

The dominant uncertainties in our model are relativistic corrections to the tidal interactions which, however, leave the qualitative conclusions about the importance of the dynamical tides for low mass ratios unaffected.

*Numerical-relativity simulations.* We produce NR simulations of nonspinning NS-BH coalescences with unprecedented length and high accuracy using the Spectral Einstein Code (SpEC) [44]. SpEC evolves Einstein's equations on a pseudospectral grid, coupled to the general relativistic equations of hydrodynamics evolved on a separate finite volume grid (which only covers regions in which matter is present) [45]. We consider mass ratios $q = m_2/m_1 = \{1, 1.5, 2, 3, 6\}$ to sample all degrees of tidal disruption. For the NS, we choose a mass $m_1 = 1.4\ M_\odot$ and radius $R_{\rm NS} = 14.4$ km, and model its EoS as a $\Gamma$-law with $\Gamma = 2$. The tidal constants for these configurations are $\lambda = 2k_2R_{\rm NS}^5/3$, $R_{\rm NS} = m_1/C_{\rm NS}$, $C_{\rm NS} = 0.1444$, $k_2 = 0.07524$, $k_3 = 0.0221$, and $M\omega_f = 0.1349(1+q)/2$ computed as in [39]. For the runs with $q = \{1, 1.5, 2\}$ we make the following improvements to SpEC with matter [10, 45]: (i) we implement higher-order (HO) finite-difference methods to evolve the fluid [46], (ii) we modify the criteria for the amount of matter leaving the outer boundary before the hydrodynamic variables are interpolated onto a larger and coarser grid, and (iii) we use a gauge [10] that is a smooth transition between a damped wave and harmonic gauge. We compute initial conditions as in Ref. [47] and achieve initial eccentricities of $\leq 5\times10^{-4}$ following Ref. [48]. All configurations are simulated at three different numerical resolutions, with $N = \{100^3, 120^3, 140^3\}$ grid points for the hydrodynamics, and target truncation errors decreased by a factor of $\sim 2$ at each resolution for the adaptive pseudospectral grid. To obtain error estimates for purely numerical effects we directly compare the phase of the NR waveforms. The mass escaping from the numerical grid gives rise to an error $\delta\phi_{dM} \approx \omega_{22}\, t\, \delta M/m_1$ [49], where we conservatively use for $\delta M$ the loss in total mass over the entire inspiral. The error due to the extrapolation of the GW signal to null infinity is computed as in [50]: we define the error as the difference between 2nd and 3rd order polynomial fits in $r^{-1}$ of the finite radius data. For the error due to the finite numerical resolution, we make a conservative estimate by assuming that for a grid spacing $\Delta x_{\rm FD}$ the error scales as $(\Delta x_{\rm FD})^2$, and, in the cases where we computed results with two hydrodynamics algorithms, the HO and a second-order (SO) method, we also include those differences in the error estimate. This leads to $\delta\phi_{\rm FD} = \alpha_{\rm FD}\max[(\phi_{\rm high} - \phi_{\rm med}), (\phi_{\rm HO} - \phi_{\rm SO})]$. The factor $\alpha_{\rm FD}$ is computed by assuming second-order convergence between the high and medium resolutions. To obtain the global error estimate we sum the errors in quadrature: $\delta\phi^2_{\rm tot} = |\delta\phi_{\rm Ext}|^2 + |\delta\phi_{\rm dM}|^2 + |\delta\phi_{\rm FD}|^2$. This is a very conservative estimate, leading to four simulations at three resolutions and using two different algorithms agreeing to much better accuracy than the error estimate. The results of the error analyses for $q=2$ are shown in Fig. 2.

*Comparing TEOB to NR.* To test the TEOB model and assess the importance of the DT effects we perform comparisons to NR simulations and to three different AT models. These models are obtained by setting in Eq. (3) $A = A_{\rm PP} + A_{\rm AT}$, with $A_{\rm AT}$ computed in the following different ways. (I) The Taylor expansion through 2PN order given in Eqs. (6.9) and (6.10) of Ref. [31] ("ad. tides 2PN"). (II) The result from the gravitational self-force (GSF) formalism, valid to linear order in the mass ratio and having the structure $A^{\rm GSF}_{\rm AT} = -3q\lambda r^{-6}[1 + 3r^{-2}(1 - r_{\rm LR}/r)^{-1} + (m_1/M)a_1(1 - r_{\rm LR}/r)^{-7/2}]$, where $a_1$ is given in Eqs. (7.24)–(7.27) of Ref. [52] ("ad. tides GSF"). The quantity $r_{\rm LR}$ is the lightring, which is at $3M$ in the test particle limit; here, however, we compute its location for the dynamics described by the TEOB model (I) following the prescription of Ref. [32]. We find that this shift of $r_{\rm LR}$ to larger values leads only to a marginal enhancement of the tidal effects. (III) A modification of (II) discussed in

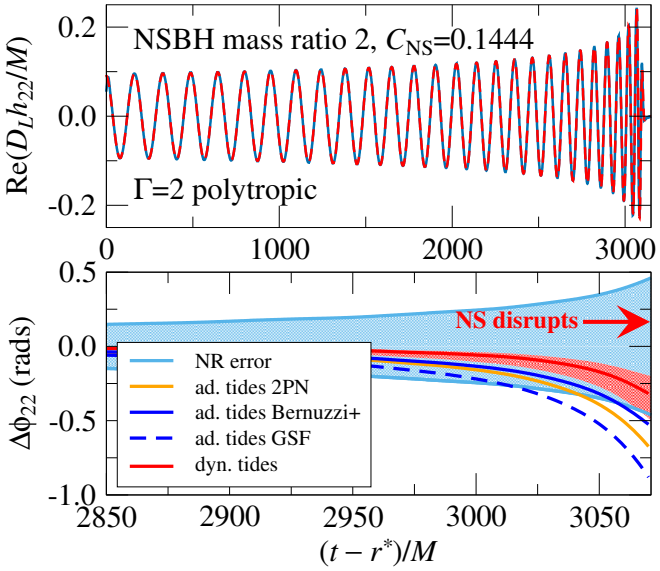


FIG. 3. **Tidal EOB models compared to NR: NS-BH coalescence with mass ratio 2**. *Upper panel*: Direct comparison of the *full* $(2,2)$ mode waveforms, aligned in phase over the first 5 initial cycles after junk radiation settles. The red curve is our TEOB model at 2PN order (Eqs. (4)), while the blue curve is the NR simulation. *Lower panel*: $(2,2)$-mode phase differences between the NR simulation and different tidal EOB models. The solid red curve shows the dephasing for the TEOB waveform presented above. The light blue shaded region indicates the NR phase error.

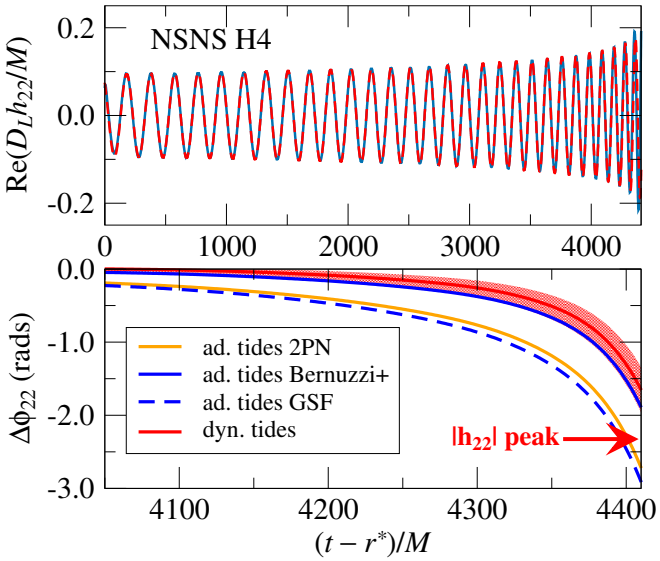


FIG. 4. **Tidal EOB models compared to NR: NS-NS coalescence for H4 EoS**. Same as Fig. 3, but now considering a NR simulation [51] of a NS-NS binary with H4 EoS, $m_1 = m_2 = 1.35 M_\odot$, and $C = 0.1470$.The estimated phase error on the NR waveform is $\sim 1$ rad at the peak in $|h_{22}|$ [51].

Ref. [32] that is obtained by adding to (II) an adjustable term $\propto (m_1/M)^2(1-r_{\rm LR}/r)^{-p}$, where $p=4$ is used ("ad. tides Bernuzzi+"). All models also include the octupole effects, using the AT result of Ref. [31] for the models described above, and, in the DT case, it is treated similar to the quadrupole [34].

The upper panel of Fig. 3 shows the NR and TEOB waveforms (using Eqs. (4)) for $q=2$; the lower panel focuses on the phase difference of the tidal models to the NR results, where the light blue shaded region spans the error of the NR data $\delta\phi_{\rm tot}$, with $\delta\phi_{\rm tot}$ computed after aligning the data over the first five GW cycles. The net size of the NS matter effects is $\sim 2$ rads as obtained by comparing to a BH-BH EOB waveform. The direct impact of DT versus only AT effects is quantified by comparing the AT 2PN results (orange curve) with the DT model (red region), where the uncertainty band is obtained from different choices for including the 2PN information as described above. As seen from Fig. 3, the inclusion of DTs in the model leads to a substantial (here $\sim 20\%$ at $t^{\rm A}_{\rm peak}$) improvement in capturing the matter effects in the late inspiral. While the overall performance of the DT model is comparable to that of the enhanced AT model (III) (solid blue curve), the key difference is that it corresponds to a solid prediction based on the underlying NS physics whereas the model (III) relies largely on an enhancement of the tidal field strength through the adjustable term, as seen by contrasting it to the GSF result (dashed blue curve).

We obtain similar results not only for the other NS-BH configurations [53] for which, however, the size of the tidal effects decreases as $\sim (1+q)^{-5}$, but also for NS-NS binaries, as shown in Fig. 4 using a NS-NS waveform from Ref. [51]. The net size of the matter effects in this case is $\sim 4$ rads, and the DT effect contributes $\sim 30\%$ of the AT phasing at the peak. Through comparisons to public BH-BH simulations [54], we verified that the phase error of the PP model is negligible ($\sim 10^{-4}$ rads) for the current discussion. These results clearly demonstrate the importance of including DT effects in robust GW template models.

*Conclusions.* We developed the first full EOB waveform model that includes dynamic instead of only adiabatic tidal effects. By comparing to new and existing NR simulations, we found compelling evidence for the significance of DT effects in both NS-BH and NS-NS inspirals, for mass ratios $\lesssim 3$ and for low NS compactnesses. In the presence of a large BH spin, preliminary estimates indicate that DT effects may remain important for mass ratios $\lesssim 5$, although the net matter effects decrease rapidly with the mass ratio. To enable robust measurements of the properties of ultradense NS matter with advanced GW detectors the DT effects must be included in GW template models. For this purpose we devised an effective description of DTs which captures the imprint of the NS matter on the inspiral GWs through both the tidal deformabilities and the $f$-mode frequencies. We completed the TEOB waveform model to cover the GWs emitted from nonspinning NS-BH mergers for all degrees of tidal disruption. Our TEOB model will be implemented for LIGO data analysis and serves as the foundation for physically more realistic cases and for

further improvements to the model.

*Acknowledgements.* We thank Kostas Kokkotas and Cole Miller for useful discussions. A.B. and T.H. acknowledge support from NSF Grant No. PHY-1208881. A.B. also acknowledges partial support from NASA Grant NNX12AN10G. T.H. thanks the Max Planck Institut für Gravitationsphysik for hospitality. Support for this work was provided by NASA through Einstein Postdoctoral Fellowship grant numbered PF4-150122 (F.F.) awarded by the Chandra X-ray Center, which is operated by the Smithsonian Astrophysical Observatory for NASA under contract NAS8-03060. M.D. acknowledges support from NSF Grant No. PHY-1402916. M.S. was supported by Grant-in-Aid for Scientific Research 24244028 of the Japanese MEXT. H.P. gratefully acknowledge support from the NSERC Canada. L.K. acknowledges support from NSF grants PHY-1306125 and AST-1333129 at Cornell, while the authors at Caltech acknowledge support from NSF Grants PHY- 1404569 and AST-1333520. Authors at both Cornell and Caltech also thank the Sherman Fairchild Foundation for their support. Computations were performed on the supercomputer Briaree from the Universite de Montreal, managed by Calcul Quebec and Compute Canada. The operation of these supercomputers is funded by the Canada Foundation for Innovation (CFI), NanoQuebec, RMGA and the Fonds de recherche du Quebec - Nature et Technologie (FRQ-NT). Computations were also performed on the Zwicky cluster at Caltech, supported by the Sherman Fairchild Foundation and by NSF award PHY-0960291. This work also used the Extreme Science and Engineering Discovery Environment (XSEDE) through allocation No. TG-PHY990007N, supported by NSF Grant No. ACI-1053575.

[1] A. W. Steiner, J. M. Lattimer, and E. F. Brown, Astrophys. J. **765**, L5 (2013), arXiv:1205.6871 [nucl-th].
[2] K. Hebeler, J. M. Lattimer, C. J. Pethick, and A. Schwenk, Astrophys. J. **773**, 11 (2013), arXiv:1303.4662 [astro-ph.SR].
[3] J. Aasi *et al.* (LIGO Scientific), Class. Quant. Grav. **32**, 074001 (2015), arXiv:1411.4547 [gr-qc].
[4] F. Acernese *et al.* (VIRGO), Class. Quant. Grav. **32**, 024001 (2015), arXiv:1408.3978 [gr-qc].
[5] Y. Aso, Y. Michimura, K. Somiya, M. Ando, O. Miyakawa, T. Sekiguchi, D. Tatsumi, and H. Yamamoto (KAGRA), Phys. Rev. **D88**, 043007 (2013), arXiv:1306.6747 [gr-qc].
[6] R. Fernández and B. D. Metzger, (2015), arXiv:1512.05435 [astro-ph.HE].
[7] K. Kawaguchi, K. Kyutoku, H. Nakano, H. Okawa, M. Shibata, and K. Taniguchi, Phys. Rev. **D92**, 024014 (2015), arXiv:1506.05473 [astro-ph.HE].
[8] J. S. Read, L. Baiotti, J. D. E. Creighton, J. L. Friedman, B. Giacomazzo, K. Kyutoku, C. Markakis, L. Rezzolla, M. Shibata, and K. Taniguchi, Phys. Rev. **D88**, 044042 (2013), arXiv:1306.4065 [gr-qc].
[9] K. Kyutoku, H. Okawa, M. Shibata, and K. Taniguchi, Phys. Rev. **D84**, 064018 (2011), arXiv:1108.1189 [astro-ph.HE].
[10] F. Foucart, M. B. Deaton, M. D. Duez, L. E. Kidder, I. MacDonald, C. D. Ott, H. P. Pfeiffer, M. A. Scheel, B. Szilagyi, and S. A. Teukolsky, Phys. Rev. **D87**, 084006 (2013), arXiv:1212.4810 [gr-qc].
[11] Z. B. Etienne, Y. T. Liu, V. Paschalidis, and S. L. Shapiro, in (2015) pp. 991–994, arXiv:1303.0837 [astro-ph.HE].
[12] L. Bildsten and C. Cutler, Astrophys. J. **400**, 175 (1992).
[13] C. S. Kochanek, Astrophys. J. **398**, 234 (1992).
[14] D. Lai, Mon. Not. Roy. Astron. Soc. **270**, 611 (1994), arXiv:astro-ph/9404062 [astro-ph].
[15] K. D. Kokkotas and G. Schäfer, Mon. Not. Roy. Astron. Soc. **275**, 301 (1995), arXiv:gr-qc/9502034 [gr-qc].
[16] E. E. Flanagan and T. Hinderer, Phys. Rev. **D77**, 021502 (2008), arXiv:0709.1915 [astro-ph].
[17] V. Ferrari, L. Gualtieri, and A. Maselli, Phys. Rev. **D85**, 044045 (2012), arXiv:1111.6607 [gr-qc].
[18] T. Damour and A. Nagar, Phys. Rev. **D79**, 081503 (2009), arXiv:0902.0136 [gr-qc].
[19] A. E. H. Love, Proceedings of the Royal Society of London Series A **82**, 73 (1909).
[20] L. Iess, R. A. Jacobson, M. Ducci, D. J. Stevenson, J. I. Lunine, J. W. Armstrong, S. W. Asmar, P. Racioppa, N. J. Rappaport, and P. Tortora, Science **337**, 457 (2012).
[21] J. Kevorkian and J. D. Cole, *Multiple scale and singular perturbation methods*, Vol. 114 (Springer Science & Business Media, 2012).
[22] M. Shibata, Prog. Theor. Phys. **91**, 871 (1994).
[23] W. C. Ho and D. Lai, Mon.Not.Roy.Astron.Soc. **308**, 153 (1999), arXiv:astro-ph/9812116 [astro-ph].
[24] E. E. Flanagan and E. Racine, Phys. Rev. **D75**, 044001 (2007), arXiv:gr-qc/0601029 [gr-qc].
[25] A. Buonanno and T. Damour, Phys. Rev. **D59**, 084006 (1999), arXiv:gr-qc/9811091 [gr-qc].
[26] A. Buonanno and T. Damour, Phys. Rev. **D62**, 064015 (2000), arXiv:gr-qc/0001013 [gr-qc].
[27] A. Taracchini *et al.*, Phys. Rev. **D89**, 061502 (2014), arXiv:1311.2544 [gr-qc].
[28] Y. Pan, A. Buonanno, A. Taracchini, L. E. Kidder, A. H. Mroué, H. P. Pfeiffer, M. A. Scheel, and B. Szilágyi, Phys. Rev. **D89**, 084006 (2014), arXiv:1307.6232 [gr-qc].
[29] T. Damour and A. Nagar, Phys. Rev. **D90**, 044018 (2014), arXiv:1406.6913 [gr-qc].
[30] A. Taracchini, Y. Pan, A. Buonanno, E. Barausse, M. Boyle, T. Chu, G. Lovelace, H. P. Pfeiffer, and M. A. Scheel, Phys. Rev. **D86**, 024011 (2012), arXiv:1202.0790 [gr-qc].
[31] D. Bini, T. Damour, and G. Faye, Phys. Rev. **D85**, 124034 (2012), arXiv:1202.3565 [gr-qc].
[32] S. Bernuzzi, A. Nagar, T. Dietrich, and T. Damour, Phys. Rev. Lett. **114**, 161103 (2015), arXiv:1412.4553 [gr-qc].
[33] J. E. Vines and E. E. Flanagan, Phys. Rev. **D88**, 024046 (2013), arXiv:1009.4919 [gr-qc].
[34] J. Steinhoff et al, in preparation (2016).
[35] K. S. Thorne, Rev. Mod. Phys. **52**, 299 (1980).
[36] T. Damour, P. Jaranowski, and G. Schaefer, Phys. Rev. **D78**, 024009 (2008), arXiv:0803.0915 [gr-qc].
[37] T. Damour, A. Nagar, and L. Villain, Phys. Rev. **D85**, 123007 (2012), arXiv:1203.4352 [gr-qc].
[38] A. Maselli, L. Gualtieri, F. Pannarale, and V. Ferrari, Phys. Rev. **D86**, 044032 (2012), arXiv:1205.7006 [gr-qc].
[39] S. Chakrabarti, T. Delsate, and J. Steinhoff, (2013), arXiv:1304.2228 [gr-qc].
[40] M. Vallisneri, Phys. Rev. Lett. **84**, 3519 (2000), arXiv:gr-qc/9912026 [gr-qc].
[41] J. A. Faber, P. Grandclement, F. A. Rasio, and K. Taniguchi, Phys. Rev. Lett. **89**, 231102 (2002), arXiv:astro-ph/0204397 [astro-ph].

[42] B. D. Lackey, K. Kyutoku, M. Shibata, P. R. Brady, and J. L. Friedman, Phys. Rev. **D89**, 043009 (2014), arXiv:1303.6298 [gr-qc].

[43] F. Pannarale, E. Berti, K. Kyutoku, B. D. Lackey, and M. Shibata, Phys. Rev. **D92**, 084050 (2015), arXiv:1509.00512 [gr-qc].

[44] http://www.black-holes.org/SpEC.html.

[45] M. D. Duez, F. Foucart, L. E. Kidder, H. P. Pfeiffer, M. A. Scheel, and S. A. Teukolsky, Phys. Rev. **D78**, 104015 (2008), arXiv:0809.0002 [gr-qc].

[46] D. Radice, L. Rezzolla, and F. Galeazzi, Class. Quant. Grav. **31**, 075012 (2014), arXiv:1312.5004 [gr-qc].

[47] F. Foucart, L. E. Kidder, H. P. Pfeiffer, and S. A. Teukolsky, Phys. Rev. **D77**, 124051 (2008), arXiv:0804.3787 [gr-qc].

[48] H. P. Pfeiffer, D. A. Brown, L. E. Kidder, L. Lindblom, G. Lovelace, and M. A. Scheel, , Class. Quant. Grav. **24**, S59 (2007), arXiv:gr-qc/0702106 [gr-qc].

[49] M. Boyle, D. A. Brown, L. E. Kidder, A. H. Mroue, H. P. Pfeiffer, M. A. Scheel, G. B. Cook, and S. A. Teukolsky, Phys. Rev. **D76**, 124038 (2007), arXiv:0710.0158 [gr-qc].

[50] M. Boyle and A. H. Mroue, Phys. Rev. **D80**, 124045 (2009), arXiv:0905.3177 [gr-qc].

[51] K. Hotokezaka, K. Kyutoku, H. Okawa, and M. Shibata, Phys. Rev. **D91**, 064060 (2015), arXiv:1502.03457 [gr-qc].

[52] D. Bini and T. Damour, Phys. Rev. **D90**, 124037 (2014), arXiv:1409.6933 [gr-qc].

[53] in preparation (2016).

[54] A. H. Mroue *et al.*, Phys. Rev. Lett. **111**, 241104 (2013), arXiv:1304.6077 [gr-qc].